193-nm photodissociation of acryloyl chloride to probe the unimolecular dissociation of CH_2CHCO radicals and CH_2CCO

D. E. Szpunar, J. L. Miller, and L. J. Butler
The James Franck Institute and Department of Chemistry, The University of Chicago, Chicago Illinois 60637

F. Qi[a)]
Chemical Sciences Division, Lawrence Berkeley National Laboratory, Berkeley, California 94720

(Received 25 September 2003; accepted 4 December 2003)

The work presented here uses photofragment translational spectroscopy to investigate the primary and secondary dissociation channels of acryloyl chloride (CH_2═$CHCOCl$) excited at 193 nm. Three primary channels were observed. Two C–Cl fission channels occur, one producing fragments with high kinetic recoil energies and the other producing fragments with low translational energies. These channels produced nascent CH_2CHCO radicals with internal energies ranging from 23 to 66 kcal/mol for the high-translational-energy channel and from 50 to 68 kcal/mol for the low-translational-energy channel. We found that all nascent CH_2CHCO radicals were unstable to CH_2CH+CO formation, in agreement with the G3//B3LYP barrier height of 22.4 kcal/mol to within experimental and computational uncertainties. The third primary channel is HCl elimination. All of the nascent CH_2CCO coproducts were found to have enough internal energy to dissociate, producing $CH_2C:+CO$, in qualitative agreement with the G3//B3LYP barrier of 39.5 kcal/mol. We derive from the experimental results an upper limit of 23 ± 3 kcal/mol for the zero-point-corrected barrier to the unimolecular dissociation of the CH_2CHCO radical to form CH_2CH+CO. © *2004 American Institute of Physics.* [DOI: 10.1063/1.1644096]

INTRODUCTION

This work investigates the primary photodissociation channels of acryloyl chloride (CH_2═$CHCOCl$) excited at 193 nm as well as the unimolecular dissociation channels of the nascent CH_2CHCO radicals and CH_2CCO molecular products formed in the primary photolysis. Acryloyl chloride is known to exist in two major conformers, the s-cis and the s-trans, as shown in Fig. 1. The s-trans is more stable than the s-cis by 0.6 kcal/mol.[1] Although many studies of acryloyl chloride have been presented in the literature, few have focused on its photochemistry. Arendt *et al.* studied the emission spectroscopy of acryloyl chloride.[2] The transition at 199 nm was identified by configuration interaction with single excitation (CIS) calculations as promotion of an electron into an orbital of π^*(C═C)/π^*(C═O) character. This assignment was supported by progressions in both the C═C and C═O stretch as well as several combination bands in the emission spectrum. Piétri *et al.*[3] studied the photolysis of argon-matrix-isolated acryloyl chloride at 10 K. At $\lambda>310$ nm, isomerization to 3-chloro-1,2-propenone (H_2ClCCH═C═O) was found to be the only pathway. At shorter wavelengths $\lambda>230$ nm, the isomerization rate was found to increase, and the resultant 3-chloro-1,2-propenone followed two subsequent dissociation pathways. The first was loss of CO to form a 2-chloroethylidene transient (H_2ClCCH:), which isomerized to vinyl chloride; the second was HCl elimination forming HCl+propadienone (CH_2═C═C═O), which absorbed another photon, producing CO+vinylidene (H_2C═C:), which isomerized to acytelene. In another study, Piétri *et al.*[4] examined the photolysis of Ar-matrix-isolated 3-chloropropanoyl chloride (CH_2ClCH_2COCl) at $\lambda>230$ nm and analyzed the results using Fourier transform infrared (FTIR) spectroscopy. One of the two major channels produced acryloyl chloride+HCl which absorbed another photon, giving the reaction $CH_2CHCOCl\rightarrow CH_2C:+CO+HCl\rightarrow HCCH+CO+HCl$.

The work presented here used photofragment translational spectroscopy to characterize the photodissociation channels of acryloyl chloride excited at 193 nm and the unimolecular dissociation channels of the nascent radicals and molecular products. Using GAUSSIAN 98,[5] we carried out G3//B3LYP calculations of the heats of reaction and barrier heights for the observed reaction channels.

EXPERIMENT

The experiments presented here were performed at the Advanced Light Source (ALS) at Lawrence Berkeley National Laboratory. The experimental apparatus has been described elsewhere.[6] Briefly, a molecular beam of acryloyl chloride was formed by bubbling He to a total backing pressure of ~725 torr through acryloyl chloride chilled to 0 °C and expanding it through a 1-mm-diam-orifice general valve at room temperature. At 0 °C, 52% of the acryloyl chloride is in the s-trans conformer. The molecular beam was intersected with the 193-nm pulsed light from a Lambda Physik LPX 220 excimer laser operating near 20 mJ/pulse. The photofragments that scattered along the detector axis flew 15.2

[a)]Current address: National Synchrotron Radiation Laboratory, University of Science and Technology of China, Hefei, Anhui 230026, China.

FIG. 1. s-trans and s-cis acryloyl chloride.

cm where they were photoionized by tunable synchrotron radiation. The resulting ions were then mass selected using a quadrupole mass filter and detected with a Daly detector.[7] The synchrotron radiation passed through an Ar filter to filter out higher harmonics for all spectra, as well as a MgF_2 window for spectra taken at a photoionization energy of 10.8 eV or less. Note that at the time these data were taken (July–November 2000), the photoionization energy was miscalibrated to the blue by approximately 0.2 eV and has recently been recalibrated. Thus the photoionization energies given in this paper are about 0.2 eV to the blue of the peak of the photon distribution. Data for all photoionization efficiency (PIE) curves shown were taken at a source angle of 20°, an aperture of 5 mm×5 mm corresponding to an ALS bandwidth ~3%, and were corrected for ALS power. The spectra shown include ion flight time, but the fits were corrected for this using an ion flight constant of 5.82 $\mu s\,(amu)^{-1/2}$. The molecular beam was characterized by aiming the beam on axis and analyzing the ''hole'' formed from the laser.

RESULTS AND ANALYSIS

We present below the data on the primary C–Cl fission and HCl elimination channels of acryloyl chloride as well as the data on the unimolecular dissociation of the nascent CH_2CHCO radicals and CH_2CCO molecular cofragments. We first give our computational results on the endoergicities and barrier heights for the channels to guide the analysis of the experimental data. Possible dissociation products upon photolysis at 193 nm are shown in reactions (1)–(4), with the heats of reaction and barrier heights calculated using the G3//B3LYP method, using GAUSSIAN 98,[5] shown in Table I. Possible subsequent decomposition channels of the nascent radical and molecular products are shown as reactions (1′), (1″), and (2′):

$$CH_2{=}CHCOCl \rightarrow CH_2CHCO + Cl, \quad (1)$$

TABLE I. Heats of reaction for reactions (1)–(4) calculated using the G3//B3LYP method. All barrier heights are zero-point corrected.

Reaction	$\Delta H^0_{0\,K}$ (kcal/mol)		Barrier height (kcal/mol)	
	s-trans reactant	s-cis reactant	s-trans reactant	s-cis reactant
(1)	81.7	83.2	-	-
(1′)	20.3	18.5	22.4	20.6
(1″)	57.3	-	56.2	-
(2)	38.2	-	-	-
(2′)	40.1	40.1	39.5	39.5
(3)	100.1	96.0	-	-
(4)	13.2	9.2	-	-

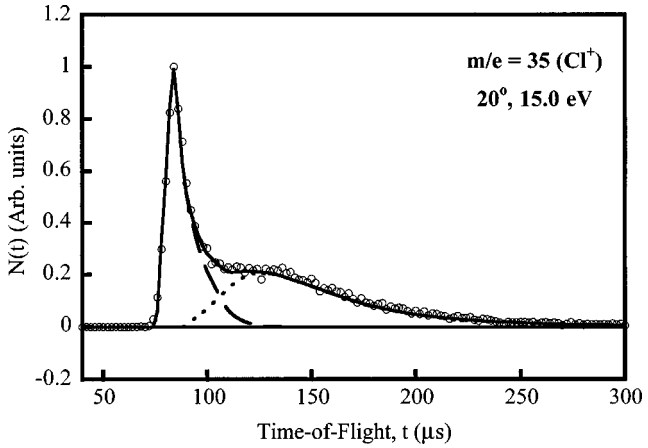

FIG. 2. Time of flight taken at $m/e=35\,(Cl^+)$ due to C–Cl bond fission, taken at a 20° source angle and a photoionization energy of 15.0 eV. The forward convolution fit to the data is broken up into two channels, which are shown in Fig. 3.

$$CH_2CHCO \rightarrow CH_2CH + CO, \quad (1')$$

$$CH_2CHCO \rightarrow CH_2CCO + H, \quad (1'')$$

$$CH_2{=}CHCOCl \rightarrow CH_2CCO + HCl, \quad (2)$$

$$CH_2CCO \rightarrow CH_2C{:} + CO, \quad (2')$$

$$CH_2{=}CHCOCl \rightarrow CH_2CH + COCl, \quad (3)$$

$$CH_2{=}CHCOCl \rightarrow CH_2CHCl + CO. \quad (4)$$

Note that the calculations suggest that reaction (1″) can proceed only through the trans conformer. This is because the loose transition-state structure closely resembles the nonlinear propadienone product (CH_2CCO). Also note that reaction (2) proceeds through the trans conformer only. Although Cl can be formed in its ground, Cl ($^2P_{3/2}$), or excited, Cl ($^2P_{1/2}$), spin-orbit state, the energy difference between the two (2.5 kcal/mol) is too small to be resolved in these experiments. Likewise, despite the listing of barrier heights and heats of formation for both conformers, they are indistinguishable given the experimental uncertainties in this study and the accuracy of the calculations. Therefore all energy calculations to follow assume s-trans acryloyl chloride reactants and Cl ($^2P_{3/2}$) products unless otherwise stated.

Figure 2 shows the data taken at $m/e=35\,(Cl^+)$ corresponding to C–Cl fission [reaction (1)]. The open circles are the experimental data and the solid line is the forward convolution fit to the data. As can be seen, the spectrum is comprised of two C–Cl fission channels. Although the exact breakdown of the translational energy distribution $[P(E_T)]$ describing C–Cl fission into two separate $P(E_T)$'s is somewhat arbitrary, it was found to be necessary to use two separate $P(E_T)$'s in order to fit the secondary dissociation products of the nascent CH_2CHCO radical. The $P(E_T)$'s derived from the forward convolution fit to the $m/e=35\,(Cl^+)$ spectrum are shown in Fig. 3. The top panel is the $P(E_T)$ derived from the forward convolution fit to the high-translational-energy C–Cl fission channel. As can be seen, it peaks near 27 kcal/mol and extends to 45 kcal/mol. The bottom panel is the $P(E_T)$ derived from the forward convolution fit to the

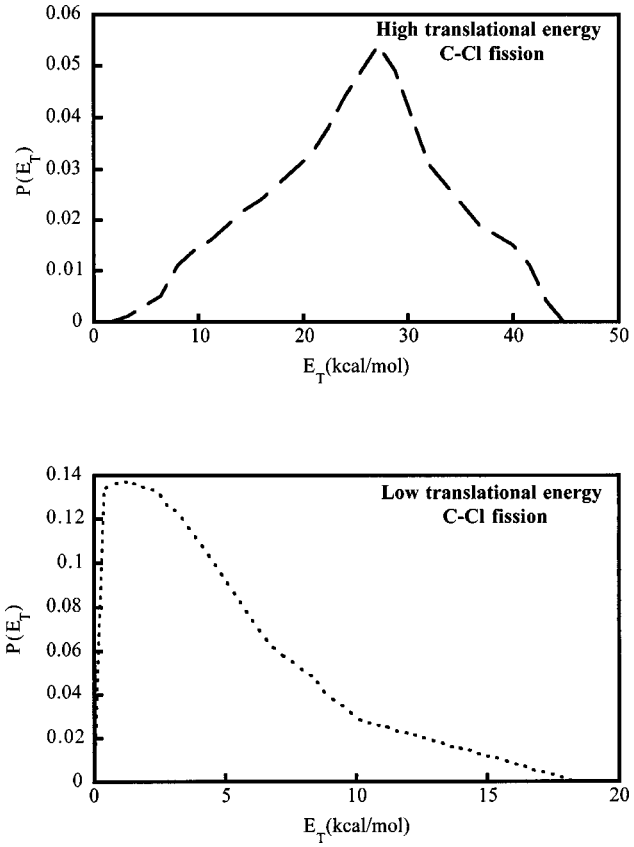

FIG. 3. Translational energy distributions used to fit the $m/e=35$ (Cl^+) data in Fig. 2. The top panel corresponds to high-translational-energy C–Cl bond fission (dashed line, Fig. 2) and the bottom panel to low-translational-energy C–Cl bond fission (dotted line, Fig. 2). All of the sibling CH_2CHCO radicals have enough energy to surmount the 22.4 kcal/mol barrier to C–CO bond fission producing CH_2CH (mass 27) + CO (mass 28). The $P(E_T)$'s shown here had to be taken into consideration when fitting the $m/e=27$ and $m/e=28$ data shown in Figs. 4 and 6, respectively, to account for the primary recoil velocity.

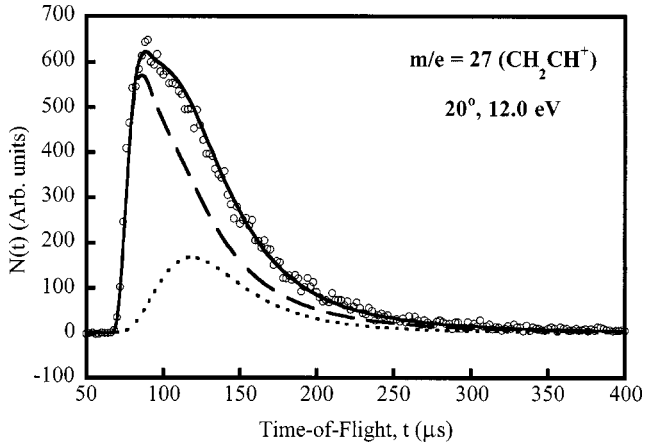

FIG. 4. Time of flight taken at $m/e=27$ (CH_2CH^+), a source angle of 20°, and a photoionization energy of 12.0 eV, corresponding to vinyl radical fragments from the dissociation of the nascent CH_2CHCO radicals. The high-translational-energy C–Cl fission contribution and low-translational-energy C–Cl fission contribution are the dashed and dotted lines, respectively. The $P(E_T)$'s derived from the forward convolution fit are shown in Fig. 5.

low-translational-energy C–Cl bond fission channel, peaking near 1 kcal/mol and extending to 18 kcal/mol. Through conservation of energy, we find that the internal energy of the nascent CH_2CHCO radical is $E_{\text{int}}=h\nu+E_{\text{vib}}-\Delta H^0_{rxn}-E_T$, where $E_{\text{vib}}=1.6$ kcal/mol is the average vibrational energy of parent acryloyl chloride calculated at the nozzle temperature of 298 K. The parent vibrational energy was calculated using G3//B3LYP frequencies scaled by 0.96, and the parent rotational energy was assumed to be negligible. This gives a range of $23<E_{\text{int}}<66$ kcal/mol for the high-translational-energy C–Cl fission channel and $50<E_{\text{int}}<68$ kcal/mol low-translational-energy C–Cl fission channel. As shown in Table I, G3//B3LYP calculations predict a barrier to $CH_2CHCO \rightarrow CH_2CH+CO$ formation [reaction (1′)] of 22.4 kcal/mol. Therefore, the majority of the nascent CH_2CHCO radicals should have enough internal energy to dissociate, producing CH_2CH (vinyl radical) + CO. In fact, no signal was found at $m/e=55$ (CH_2CHCO^+) after 40 000 shots taken at a source angle of 10° and an ionization energy of 8.5 eV, 60 000 shots at a source angle of 7° and an ionization energy of 12.0 eV, and 50 000 shots at a source angle of 7° and an ionization energy of 8.5 eV, suggesting that all of the nascent CH_2CHO radicals do indeed surmount the barrier to secondary dissociation. This is within the accuracy of G3//B3LYP calculations (±2 kcal/mol) as well as experimental uncertainties. We detect the unimolecular dissociation products, CH_2CH+CO [reaction (1′)] of the nascent CH_2CHCO radicals at $m/e=27$ (CH_2CH^+) and 28 (CO^+). Data taken at $m/e=27$ [CH_2CH^+, reaction (1′)], a source angle of 20°, and an ionization energy of 12.0 eV are shown in Fig. 4. Note that the recoil velocity from the primary photolysis event [$P(E_T)$'s shown in Fig. 3] had to be incorporated in the fit of these data. In this as well as all other secondary dissociation channels, a standard forward convolution fitting program was used, with the $P(E_T)$ derived from the forward convolution fit to the corresponding primary reaction entered to account for primary recoil velocity and the $P(E_T)$ for the secondary fission channel iteratively changed to fit the data. The dashed line contribution in Fig. 4 is due to CH_2CH fragments from the dissociation of the nascent CH_2CHCO radical formed in the high-translational-energy C–Cl fission process (dashed line in Fig. 2, top panel in Fig. 3). The dotted line is due to the CH_2CH contribution from the secondary dissociation of the low-translational-energy C–Cl fission CH_2CHCO products (dotted line in Fig. 2, bottom panel in Fig. 3). The translational energy distributions for the unimolecular dissociation of CH_2CHCO derived from the forward convolution fit to the data are shown in Fig. 5. The top panel shows the distribution of recoil kinetic energies for C–C fission of the CH_2CHCO radical produced in the C–Cl primary photolysis channel forming high relative velocities of the Cl atom and the CH_2CHCO radical (and correspondingly lower internal energy CH_2CHCO radicals). The bottom panel shows the distribution of recoil kinetic energies for C–C fission of the CH_2CHCO radicals formed from the C–Cl primary photolysis channel products with low relative velocities. It is interesting to note that C–C fission of the lower internal energy radicals actually partitions more energy to the $CO+C_2H_3$ product recoil than C–C fission of the higher-internal-energy group of radicals. We return to

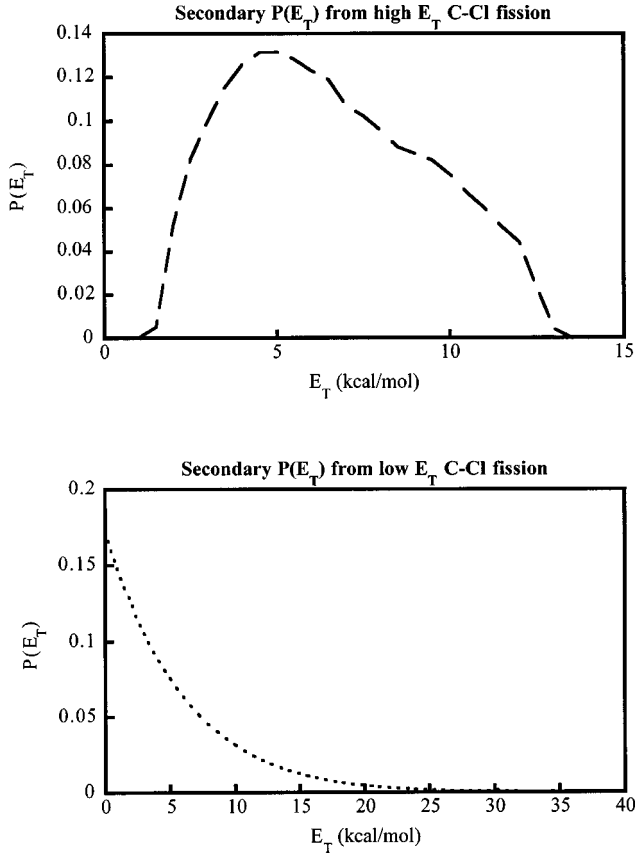

FIG. 5. Translational energy distributions used to fit the $m/e=27\,(CH_2CH^+)$ data in Fig. 4. The top panel corresponds to secondary dissociation from the high-translational-energy C–Cl bond fission CH_2CHCO radicals (dashed line, Fig. 2) and the bottom panel to low-translational-energy C–Cl bond fission CH_2CHCO radical dissociation (dotted line, Fig. 2). The $P(E_T)$'s shown in Fig. 3 had to be taken into consideration in fitting of the $m/e=27$ spectrum to account for the primary recoil velocity.

this in the Discussion. Data were also collected at $m/e=28\,(CO^+)$, corresponding to the momentum-matched partner of C_2H_3 in reaction (1′). Figure 6 shows $m/e=28\,(CO^+)$ data taken at a source angle of 20° and a photoionization energy of 15.0 eV. The dashed line corresponds to the fit to the CO products from the dissociation of nascent CH_2CHCO radicals produced in the high-translational-energy C–Cl fission channel, again using the secondary $P(E_T)$ shown in the top panel of Fig. 5. The dotted line in Fig. 6 corresponds to CO products from the dissociation of nascent CH_2CHCO radicals produced in the low-translational-energy C–Cl fission channel products [secondary $P(E_T)$ shown in the bottom panel of Fig. 5]. The dash-dotted line contribution is attributed to CO products formed in the dissociation of nascent CH_2CCO products from HCl elimination [reaction (2′), $P(E_T)$ shown in Fig. 11] and will be discussed shortly. We do not include contributions from dissociative ionization from mass-55 (CH_2CHCO) or mass-54 (CH_2CCO) products in the fit shown because the calculated energetics and primary product $P(E_T)$ distributions indicate that the CH_2CHCO or CH_2CCO products should have, in fact, all undergone secondary dissociation in the interaction region. A photoionization efficiency curve of

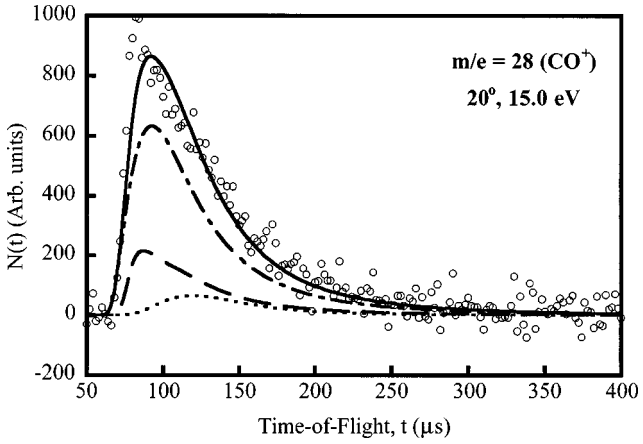

FIG. 6. Time of flight taken at $m/e=28\,(CO^+)$, a source angle of 20°, and a photoionization energy of 15.0 eV, corresponding to carbon monoxide fragments from the dissociation of the nascent CH_2CHCO radicals. The high-translational-energy C–Cl fission contribution and low-translational-energy C–Cl fission contribution are the dashed and dotted lines, respectively, and the dot-dashed line is due to secondary dissociation of the nascent CH_2CCO product formed from HCl elimination. The $P(E_T)$'s derived from the forward convolution fit are shown in Fig. 5 for the C–Cl elimination contribution and Fig. 11 for the HCl elimination contribution.

$m/e=27\,(C_2H_3^+)$ is shown in Fig. 7. The MgF_2 filter was in place for all data in the PIE curve. The appearance of signal near 8.5 eV compares well to the 8.25 eV vinyl radical ionization energy.[8] This PIE curve is qualitatively similar to the $m/e=27\,(C_2H_3^+)$ PIE curve of vinyl radicals produced through the 193-nm photolysis of vinyl chloride.[9]

Figure 8 shows the data taken at $m/e=36\,(HCl^+)$ corresponding to primary HCl elimination [reaction (2)] upon photolysis of acryloyl chloride at 193 nm, a channel that competes with the C–Cl fission channel. The $P(E_T)$ derived from the forward convolution fit to the data peaks near 5 kcal/mol and extends to 49 kcal/mol, as shown in Fig. 9. This leaves the nascent propadienone products (CH_2CCO) and

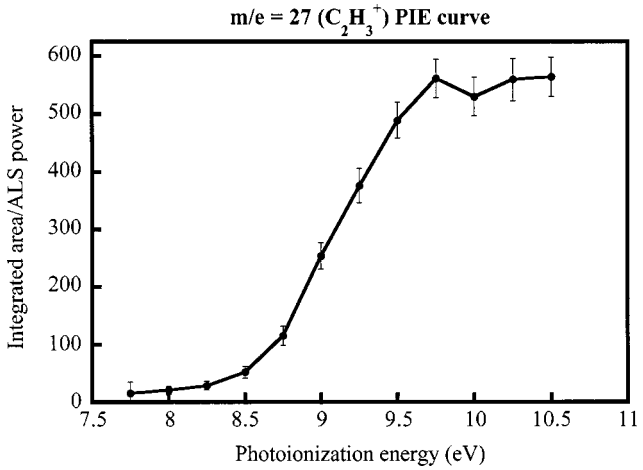

FIG. 7. Photoionization efficiency (PIE) curve for the $m/e=27\,(C_2H_3^+)$ products formed from the secondary dissociation of the CH_2CHCO radicals produced from C–Cl fission. Each point is the integrated area from 60 to 300 μs of signal accumulated for 20 000 shots (corrected for ALS power), with a source angle of 20°. The data points are shown with error bars and with straight-line extrapolations to guide the eye. All data shown were taken with the MgF_2 window.

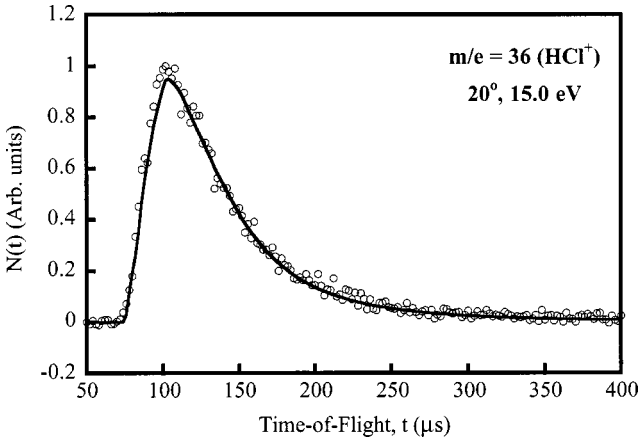

FIG. 8. Time of flight taken at $m/e=36$ (HCl^+), a 20° source angle, and a photoionization energy of 15.0 eV. The $P(E_T)$ derived from the forward convolution fit is shown in Fig. 9.

HCl fragments with internal energies in the range $62<E_{\text{int}}<111$ kcal/mol. Depending on how this internal energy is distributed between the HCl and propadienone products, some or all of the nascent propadienone may have more internal energy than the 40.1-kcal/mol barrier to $CH_2{=}{=}C$: (vinylidene) + CO formation [reaction (2′)]. There was no signal observed at $m/e=54$ (CH_2CCO^+) after 50 000 shots taken at a source angle of 10° and a photoionization energy of 10.8 eV. Data were collected at $m/e=26$ ($C_2H_2^+$) and $m/e=28$ (CO^+) corresponding to the products formed from secondary dissociation of nascent CH_2CCO products [reaction (2′)]. The time-of-flight spectrum collected at $m/e=26$ ($C_2H_2^+$), a source angle of 20°, and a photoionization energy of 14.0 eV is shown in Fig. 10. The data are fit assuming secondary dissociation of all of the nascent propadienone fragments resulting from HCl elimination. Once again,

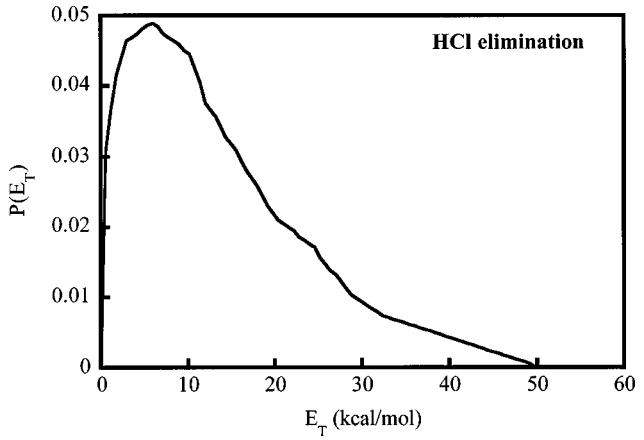

FIG. 9. Translational energy distribution derived from the forward convolution fit to $m/e=36$ (HCl^+) describing HCl elimination shown in Fig. 8. Up to 50 kcal/mol is partitioned to translational energy, leaving the HCl and CH_2CCO (propadienone) products with greater than 60.4 kcal/mol. All of the CH_2CCO products were found to have enough internal energy to overcome the 40.1-kcal/mol barrier to $CH_2C:+CO$ production. This $P(E_T)$ had to be taken into consideration when fitting the $m/e=26$ ($C_2H_2^+$) and $m/e=28$ (CO^+) data corresponding to the secondary dissociation of the nascent propadienone fragments (data shown in Figs. 10 and 6, respectively) to account for the primary recoil velocity.

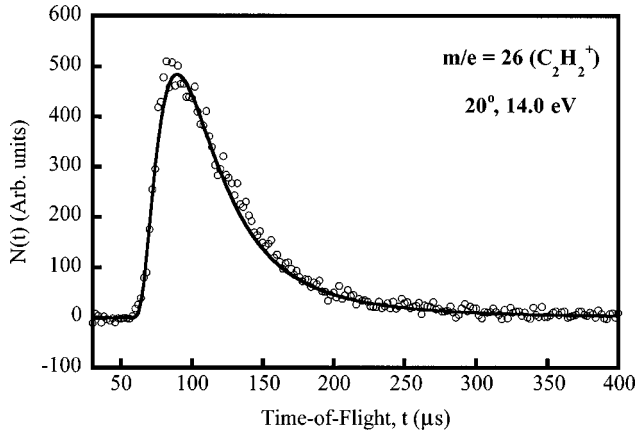

FIG. 10. Time of flight taken at $m/e=26$ ($C_2H_2^+$) at a source angle of 20° and a photoionization energy of 14.0 eV. The $m/e=26$ signal arises from the dissociation of the nascent CH_2CCO fragments produced in the HCl elimination channel. It was found that all of the CH_2CCO products had enough internal energy to overcome the 40.1 kcal/mol barrier to $CH_2C:+CO$ production. The $P(E_T)$ describing HCl elimination (Fig. 9) had to be taken into account in the fitting of this data to account for the primary recoil velocity and is shown in Fig. 11.

the recoil velocity imparted in the primary photolysis step (Fig. 9) must be taken into account in the forward convolution fit to the $m/e=26$ data. The $P(E_T)$ for the C–C fission channel of the nascent CH_2CCO products derived from the forward convolution fit is shown in Fig. 11. As can be seen, it peaks near 6 kcal/mol and extends to 44 kcal/mol. We have used the assumption that the secondary dissociation of all propadienone products is represented by the same recoil kinetic energy distribution, as obtaining a good fit to the data did not require otherwise. To help determine the partitioning of internal energy to the HCl fragment, a PIE curve taken at $m/e=36$ was taken and is shown in Fig. 12. As all data shown were taken at ionization energies greater than 10.8 eV, the MgF_2 filter was not used. A PIE curve was taken at $m/e=26$ ($C_2H_2^+$) and is shown in Fig. 13. For this PIE

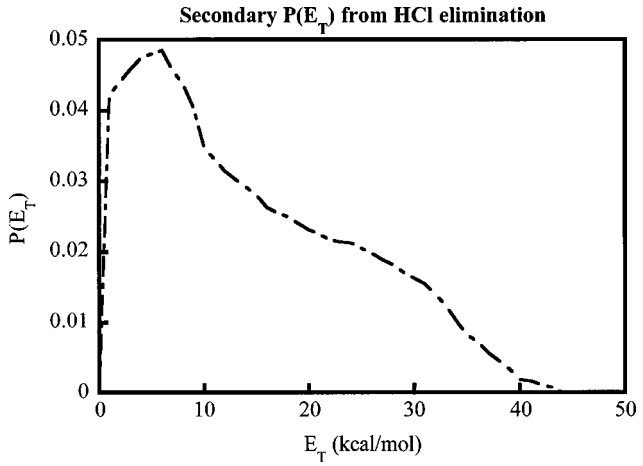

FIG. 11. Translational energy distribution derived from the forward convolution fit to the $m/e=26$ ($C_2H_2^+$) data shown in Fig. 10, formed through the dissociation of CH_2CCO fragments produced in the HCl elimination channel. Note that the velocity imparted in the HCl elimination channel had to be taken into account [$P(E_T)$ shown in Fig. 9] in the forward convolution fit of the $C_2H_2^+$ data.

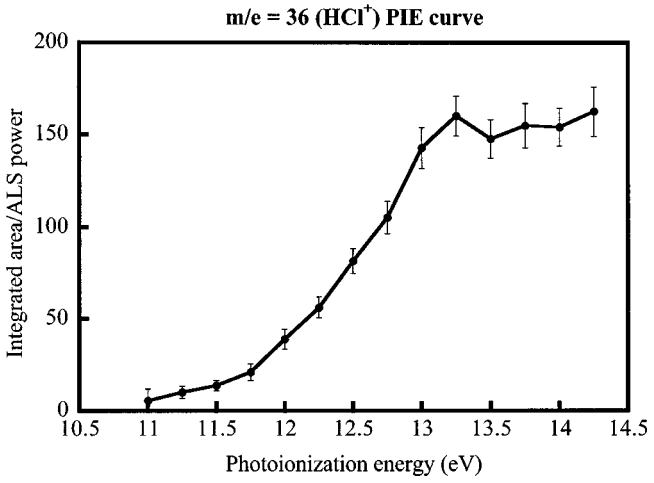

FIG. 12. Photoionization efficiency (PIE) curve for the $m/e=36\,(HCl^+)$ products formed from acryloyl chloride HCl elimination. Each point is the integrated area from 60 to 280 μs of signal accumulated for 10 000 shots (corrected for ALS power), with a source angle of 20°. The data points are shown with error bars and with straight-line extrapolations to guide the eye. All data shown were taken without the MgF_2 window.

curve, the MgF_2 filter was in place for the spectra taken at a photoionization energy less than 10.8 eV and not used for photoionization energies greater than 10.8 eV. To normalize for this, the point in Fig. 13 at 10.75 eV is the 10.75-eV data point taken without the filter and normalized to the data taken with the filter. We will return to the PIE curves in the Discussion.

The dot-dashed line contribution shown in the $m/e=28\,CO^+$ time of flight in Fig. 6 corresponds to the momentum-matched CO partner of the C_2H_2 product in reaction (2′). In the fit shown, the ratio, appropriately corrected for kinematic factors, between the CO products produced by

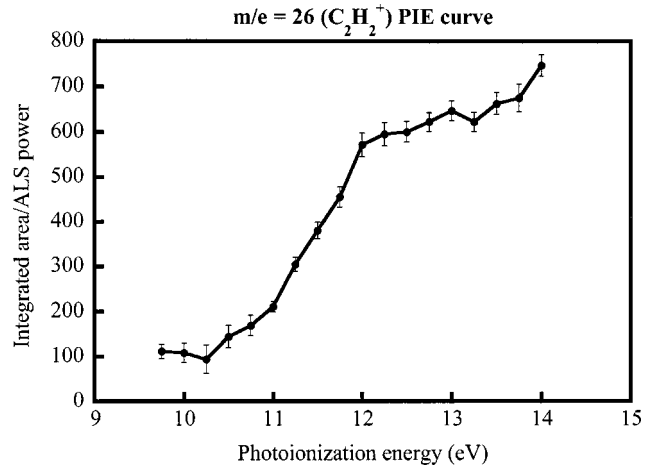

FIG. 13. Photoionization efficiency (PIE) curve for the $m/e=26\,(C_2H_2^+)$ products formed from the dissociation of nascent CH_2CCO fragments formed from HCl elimination. Each point is the integrated area from 50 to 400 μs of signal accumulated for 20 000 shots (corrected for ALS power), with a source angle of 20°. The data points are shown with error bars and with straight-line extrapolations to guide the eye. The data collected at energies less than 10.75 eV used the MgF_2 filter and those above 10.75 eV did not. Data at 10.75 eV are the normalized signal taken with and without the MgF_2 filter.

secondary dissociation of C–Cl fission products [reaction (1′), dotted and dashed lines] and the CO products produced by secondary dissociation of propadienone resulting from HCl elimination [reaction (2′), dot-dashed line] is 0.34:1. A ratio of 0.68:1 also gave a similar fit to the data. Though one might be tempted to use these ratios to give a crude estimate of the branching between channel 1 (C–Cl fission) and channel 2 (HCl elimination) in acryloyl chloride, we do not believe a reliable branching ratio may be determined in this way. Not only is the fit fairly insensitive to the ratio used, but also the fast signal in the data in Fig. 6 near 80 μs is not adequately fit with any trial ratio. This signal cannot be fit by the assumption that the fastest CH_2CHO radicals survived secondary dissociation, so it is most likely due to an unidentified multiphoton process. A more reliable estimate of the C–Cl fission/HCl elimination absolute branching ratio might be obtained by integrating the Cl^+ and HCl^+ time-of-flight data and using the following equation:

$$\frac{\mathrm{Cl}}{\mathrm{HCl}}=\frac{N_{\mathrm{Cl}^-}}{N_{\mathrm{HCl}^+}}\frac{\mathrm{TS}_{\mathrm{Cl}^+}}{\mathrm{TS}_{\mathrm{HCl}^+}}\frac{Q_{\mathrm{HCl}}}{Q_{\mathrm{Cl}}}\frac{f_{\mathrm{HCl}}}{f_{\mathrm{Cl}}},$$

$$\frac{\mathrm{Cl}}{\mathrm{HCl}}=\frac{26679.4/36}{16683.4/37}\frac{36.99}{24.53}\frac{56}{43.6}\frac{1}{1}=3.18, \tag{5}$$

where N_x is the integrated area of the time of flight taken at the corresponding fragment ($m/e=35$, Cl^+; $m/e=36$, HCl^+) in an equal number of laser shots, normalized for ALS flux (36 mW for Cl, 37 mW for HCl, both taken at 15.0 eV), TS_x is the theoretical scaling factor (accounting for Jacobian factors in the conversion from center-of-mass trail to laboratory scattering frames, transit time through the ionizer, flux measured in time versus kinetic energy space and angular and velocity distributions of the scattered photofragments), Q_y is the photoionization cross section of species y, and f_y accounts for daughter ion fragmentation of species y. The photoionization cross sections for Cl (Ref. 10) and HCl (Ref. 11) are known, and f_{Cl} is unity. Because the HCl data were taken at a photoionization energy of 15.0 eV, which should still be in the flat region of the PIE curve of HCl (Fig. 14), f_{HCl} was taken as unity as well. Equation (5) gives a value of Cl/HCl=3:1. This estimate is only approximate, so we can only say that C–Cl bond fission is the more probable reaction channel.

No signal was seen at $m/e=63$ [$COCl^+$, reaction (3)], at a source angle of 10° and a photoionization energy of 10.8 eV over 50 000 shots, at a 15° source angle and a photoionization energy of 14.5 and 13.0 eV over 50 000 shots, and at a source angle of 7° and a photoionization energy of 13.0 eV over 30 000 shots. There was also no signal observed at $m/e=62\,(CH_2CHCl^+)$ corresponding to reaction (4), when taken at a source angle of 10° and a photoionization energy of 10.8 eV over 50 000 shots and at a source angle of 7° and a photoionization energy of 13.0 eV over 50 000 shots. As mentioned in the HCl elimination discussion, no signal was found at $m/e=54\,(CH_2CCO^+)$, showing no evidence for C–H fission of the nascent CH_2CHCO radical [reaction (1″)].

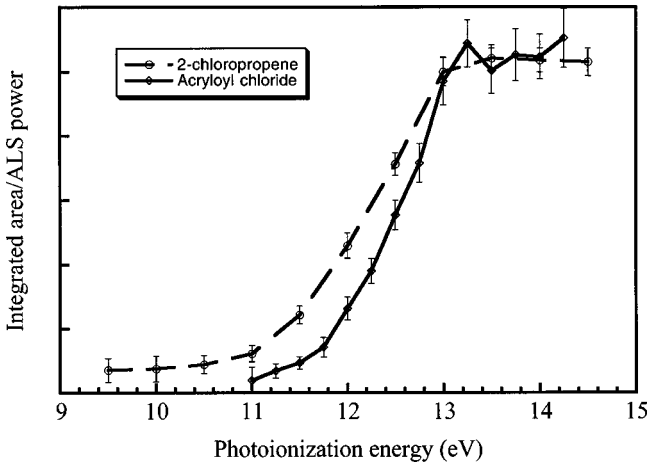

FIG. 14. Comparison of $m/e=36\,(HCl^+)$ photoionization efficiency (PIE) curves from 2-chloropropene (dashed line) and acryloyl chloride (solid line). The acryloyl chloride PIE curve has been scaled to the 2-chloropropene PIE curve to facilitate comparison. The 2-chloropropene PIE curve is reproduced with permission from Fig. 14, Ref. 13.

DISCUSSION

Acryloyl chloride excited at 193 nm was found to undergo three major primary dissociation channels leading to two sets of chemical products. The first two result from C–Cl fission, one producing high-translational-energy products and the other producing low-translational-energy products. The presence of two C–Cl bond fission channels is analogous to C–Cl bond fission of other systems involving a $\pi\rightarrow\pi^*$ transition, such as allyl chloride[12] and 2-chloropropene.[13] The high-translational-energy channel most likely arises from an electronic predissociation via a state repulsive in the C–Cl bond, as seen in the other systems.[12,13] It is possible that the low-translational-energy channel results from C–Cl fission following internal conversion to the ground electronic state. Time of flights measured at $m/e=35\,(Cl^+)$ determine that the nascent CH_2CHCO radicals have greater than 23 kcal/mol of internal energy, assuming Cl ($^2P_{3/2}$) formation. It was found that all of these radicals undergo secondary dissociation to form vinyl radicals (CH_2CH) and CO [reaction (1′)]. Within the experimental uncertainties and computational accuracy, this agrees with the G3//B3LYP 22.4 kcal/mol barrier to reaction (1′). The $P(E_T)$ describing C–C fission of the radicals from the low-translational-energy C–Cl fission channel was fit using a statistical translational energy distribution generated from an RRKM calculation[14] using the G3//B3LYP frequencies and moments of inertia at the transition state. The $P(E_T)$ used was a weighted sum of $P(E_T)$'s generated at CH_2CHCO internal energies of 63.6, 60.8, 55.2, and 50.4 kcal/mol with weightings of 1, 0.8, 0.25, and 0.1, respectively (weightings are proportional to their probability). The $P(E_T)$ describing C–C fission in the radicals from the high-translational-energy C–Cl fission channel peaks near 5 kcal/mol, significantly larger than the calculated barrier of 2.1 kcal/mol to the CH_2CH+CO reverse reaction on the ground-state potential energy surface. It is possible that high-translational-energy C–Cl fission produces an electronically excited $\dot{C}H_2CH{=}C{=}O$ radical rather than the $\tilde{X}(^2A')$ ground-state $CH_2{=}CH\dot{C}{=}O$ radical, which then experiences a larger exit barrier when it dissociates. Although the dissociation channel of the higher-energy $^2A''$ $\dot{C}H_2CH{=}C{=}O$ radical might have a larger reverse barrier than the 2.1-kcal/mol barrier to dissociation of the $\tilde{X}(^2A')$ radical, this radical is calculated[15] at the QCISD/6-311G(d,p) level of theory with zero-point corrections to be only 0.33 kcal/mol higher in energy than the ground-state $\tilde{X}(^2A')$ s-trans radical. Though Ref. 15 gives a barrier of only 2.7 kcal/mol between the ground-state $\tilde{X}(^2A')$ s-trans radical and higher-energy $^2A''$ radical, we note that this barrier is at a conical intersection, so rapid conversion between the two radicals may be suppressed. Because no signal was found at $m/e=54\,(CH_2CCO^+)$, C–H bond fission of the CH_2CHCO radical to produce CH_2CCO [reaction (1″)] was found not to compete with C—CO bond fission, as expected from the calculated barrier heights alone.

The third major channel is HCl elimination, which produces the nascent HCl+propadienone fragments with internal energies greater than 60 kcal/mol. Propadienone is known to dissociate readily to form $CH_2C{:}+CO$ [reaction (2′)].[16] Therefore, if at least 39 kcal/mol of this available internal energy is distributed to the propadienone (CH_2CCO) fragment, it should dissociate. The PIE curve in Fig. 12 can provide a rough estimate of the amount of internal energy partitioned to the HCl fragment. The appearance of signal well before the 12.75-eV ionization energy of HCl signals the partitioning of considerable internal energy to the HCl fragment. The observed redshift is on the order of 1 eV (23 kcal/mol). If this is used as a rough determination of HCl internal energy, it leaves the nascent propadienone fragments with greater than 37 kcal/mol of internal energy, which is qualitatively near the 39.5-kcal/mol barrier to C–CO fission. Our data show that all of the nascent propadienone fragments underwent C—C bond fission to produce $CH_2C{:}+CO$, in agreement with the above prediction. The barrier to $CH_2C{:}\rightarrow CH{\equiv}CH$ rearrangement is predicted to be 1.5 kcal/mol,[17] so the rearrangement should occur readily. A concerted reaction for propadienone to directly produce $HCCH+CO$ has been proposed,[18] but the supposition was created to explain C_2H_2+CO products formed despite an earlier vinylidene-acetylene isomerization barrier height of 8.6 kcal/mol.[19] Our attempts to find such a concerted transition state at the G3//B3LYP level of theory failed. Using the $m/e=26\,(C_2H_2^+)$ PIE curve shown in Fig. 13, it is not possible to distinguish between the two C_2H_2 isomers, as the ionization energies are too similar (11.4 for acetylene[8] and 11.37 eV for vinylidene,[20] respectively). Based on the thermodynamic stability of acetylene compared to $CH_2C{:}$ and the low barrier to isomerization, the dominant C_2H_2 fragment is most likely acetylene.

One might also consider 1–3 chlorine migration of acryloyl chloride to form 3-chloro-1,2-propenone, as seen by Piétri *et al.*[3] The barrier to this isomerization channel was calculated using the G3//B3LYP method to be 44.3 kcal/mol. As this is higher than the HCl elimination barrier of ~38 kcal/mol, it should not compete effectively. However, as the dis-

sociation channels of 3-chloro-1,2-propenone are the same as those of acryloyl chloride, it is not possible to entirely rule out isomerization to 3-chloro-1,2-propenone.

It is interesting to compare the $m/e=36$ (HCl^+) PIE curve (Fig. 12) with that from HCl elimination of 2-chloropropene excited at 193 nm.[13] Both acryloyl chloride and 2-chloropropene feature four-center HCl eliminations with similar transition-state HCl bond lengths (1.907 and 1.897 Å for propyne and allene formation from 2-chloropropene HCl elimination[21] [B3LYP/6-31G(d)] compared to 1.85 Å for acryloyl chloride HCl elimination). The assumption that the HCl bond length at the transition state determines the vibrational excitation of the HCl product in both 2-chloropropene and vinyl chloride HCl elimination was used to explain the similarity between $m/e=36$ PIE curves from HCl elimination from 2-chloropropene and vinyl chloride.[21] Extending this thinking, one would predict similar acryloyl chloride and 2-chloropropene $m/e=36$ PIE curves, with the HCl from acryloyl chloride being slightly blueshifted, as it has a slightly shorter H–Cl distance at the transition state. Figure 14 shows the PIE curve from Fig. 12 plotted alongside the $m/e=36$ PIE curve from HCl elimination of 2-chloropropene.[13] Indeed, the 2-chloropropene PIE curve (dashed line) is slightly more redshifted and has a lower rise than that of acryloyl chloride (solid line). These PIE curves, attributed to four-center elimination, are significantly redshifted from the PIE curve of HCl produced from allyl chloride excited at 193 nm, which could result from a three-center elimination.[12]

ACKNOWLEDGEMENTS

This work was supported by the Division of Chemical Sciences, Office of Basic Energy Sciences, Office of Energy Research, U.S. Department of Energy, under Grant No. DE-FG02-92ER14305 (L.J.B.). The Chemical Dynamics Beamline is supported by the Director, Office of Science, Office of Basic Energy Sciences, Chemical Sciences Division of the U.S. Department of Energy under Contract No. DE-AC03-76SF00098. The ALS facility is supported by the Director, Office of Science, Office of Basic Energy Sciences, Materials Sciences Division of the U.S. Department of Energy, under the same contract.

[1] W. R. Feairheller and J. E. Katon, J. Chem. Phys. **47**, 1248 (1967).
[2] M. F. Arendt, P. W. Browning, and L. J. Butler, J. Chem. Phys. **103**, 5877 (1995).
[3] N. Pietri, M. Monnier, and J.-P. Aycard, J. Org. Chem. **63**, 2462 (1998).
[4] N. Pietri, J. Piot, and J.-P. Aycard, J. Mol. Struct. **443**, 163 (1998).
[5] M. J. Frisch, G. W. Trucks, H. B. Schlegel *et al.*, GAUSSIAN 98, revision A.11.3, Gaussian, Inc., Pittsburgh, PA, 2002.
[6] X. Yang, J. Lin, Y. T. Lee, D. A. Blank, A. G. Suits, and A. M. Wodtke, Rev. Sci. Instrum. **68**, 3317 (1997).
[7] N. R. Daly, Rev. Sci. Instrum. **31**, 264 (1960).
[8] *NIST Chemistry WebBook, NIST Standard Database Number 69* (National Institute of Standards and Technology, Gaithersburg, MD, 2001).
[9] D. A. Blank, W. Sun, A. G. Suits, Y. T. Lee, S. W. North, and G. E. Hall, J. Chem. Phys. **108**, 5414 (1998).
[10] J. A. R. Samson, Y. Shefer, and G. C. Angel, Phys. Rev. Lett. **56**, 2020 (1986).
[11] J. W. Gallagher, C. E. Brion, J. A. R. Samson, and P. W. Langhoff, J. Phys. Chem. Ref. Data **17**, 9 (1988).
[12] M. L. Morton, L. J. Butler, T. A. Stephenson, and F. Qi, J. Chem. Phys. **116**, 2763 (2002).
[13] J. A. Mueller, B. F. Parsons, L. J. Butler, F. Qi, O. Sorkhabi, and A. G. Suits, J. Chem. Phys. **114**, 4505 (2001).
[14] W. L. Hase and D. L. Bunker, a general RRKM program, 1974 QCPE 234.
[15] A. L. Cooksy, J. Phys. Chem. A **102**, 5093 (1998).
[16] R. F. C. Brown, F. W. Eastwood, and G. L. McMullen, Aust. J. Phys. **30**, 179 (1977).
[17] N.-y. Chang, M.-y. Shen, and C.-h. Yu, J. Chem. Phys. **106**, 3237 (1997).
[18] L. Radom, Aust. J. Phys. **31**, 1 (1978).
[19] C. E. Dykstra and H. F. Schaefer, J. Am. Chem. Soc. **100**, 1378 (1978).
[20] B. S. Jursic, Int. J. Quantum Chem. **72**, 571 (1999).
[21] B. F. Parsons, L. J. Butler, and B. Ruscic, Mol. Phys. **100**, 865 (2002).